

Observation of nonreciprocal directional dichroism via electromagnon resonance in a chiral-lattice helimagnet $\text{Ba}_3\text{NbFe}_3\text{Si}_2\text{O}_{14}$

H. Narita,^{1,*} Y. Tokunaga,^{2,3} A. Kikkawa,³ Y. Taguchi,³ Y. Tokura,^{1,3} and Y. Takahashi^{1,3,4}

¹*Department of Applied Physics and Quantum Phase Electronic Center, University of Tokyo, Tokyo 113-8656, Japan*

²*Department of Advanced Materials Science, University of Tokyo, Kashiwa 277-8561, Japan*

³*RIKEN Center for Emergent Matter Science (CEMS), Wako 351-0198, Japan*

⁴*PRESTO, Japan Science and Technology Agency, Chiyoda, Tokyo 102-8666, Japan*

(Received 9 July 2016; revised manuscript received 26 August 2016; published 26 September 2016)

Nonreciprocal directional dichroism (NDD) is investigated on a magnetic resonance with both electric and magnetic dipole activities, i.e., electromagnon, for a chiral-lattice helimagnet $\text{Ba}_3\text{NbFe}_3\text{Si}_2\text{O}_{14}$ by terahertz spectroscopy under the magnetic field. In the Voigt geometry, the electromagnon resonance causes the NDD in the helimagnetic phase in accord with the spin-driven ferroelectric polarization, whose polarity is uniquely selected owing to the structural chirality. In the Faraday geometry, all possible optical effects, including natural optical activity, magnetic optical activity and magnetochiral effect showing NDD, are separately evaluated by terahertz polarimetry technique. The NDD is manifested in the electromagnon resonance in the helimagnetic phase, while a formation of helimagnetic spin structure enhances the natural optical activity inherent to the structural chirality.

DOI: [10.1103/PhysRevB.94.094433](https://doi.org/10.1103/PhysRevB.94.094433)

I. INTRODUCTION

The concept of chirality has been playing important roles in broad research fields including physics, chemistry, biology, and optics [1]. Chiral atomic arrangement or structural chirality in solids is potentially coupled with magnetism, leading to noncollinear spin orders such as helimagnetism. Recently, the helimagnetism in chiral magnets has attracted increasing attention for skyrmions [2,3] and chiral solitons [4] as well as for magnetoelectric (ME) multiferroics [5–7], in which the helical spin order produces ferroelectricity [8]. One representative microscopic mechanism for the spin-driven ferroelectricity is described by the spin-current (SC) model [9] or inverse Dzyaloshinskii-Moriya (DM) interaction [10,11]; the local electric polarization \mathbf{p} of which can be expressed as $\mathbf{p} \propto \mathbf{e}_{ij} \times (\mathbf{S}_i \times \mathbf{S}_j)$, where \mathbf{e}_{ij} is the unit vector connecting the adjacent spins, \mathbf{S}_i and \mathbf{S}_j . Therefore, a cycloidal spin structure generates the macroscopic electric polarization \mathbf{P} , where the helicity of spins is responsible for the sign of \mathbf{P} . For example, a proper screw-spin structure [see Fig. 1(a)] is transformed into a transverse conical spin structure by a magnetic field, resulting in ferroelectric polarization perpendicular to the magnetic field owing to the appearance of the cycloidal spin component, as shown in Fig. 1(b) [12]. The important feature of structurally chiral or chiral-lattice helimagnets is that the sign of ferroelectric polarization induced by the external magnetic field is spontaneously and uniquely selected without any external electric field; the crystal with single-handedness tends to form a single magnetic-helicity domain, i.e., either right-handed or left-handed helical spin structure.

In addition to the ME coupling in the ground state, the helimagnets also exhibit novel dynamical ME responses to an electromagnetic field, i.e., the optical ME (OME) effect [13,14]. These OME effects are exemplified by the

nonreciprocal directional birefringence/dichroism (NDD); the counter-propagating light beams undergo different optical responses. Since the OME effect is generic for the matter under the simultaneous breaking of both time-reversal and space-inversion symmetries, directional birefringence/dichroism has been reported in various types of matter such as solids [15–23], molecules [24–27], gases [28], and artificial materials [29], as well as in a broad frequency range spanning the microwave, terahertz, near-infrared, and x-ray regimes. However, an appreciable magnitude of directional dichroism is still rare, except for the magnetic excitations in the ME multiferroics. Above all, the helimagnets always provide strong ME coupling in the electromagnon resonance, which is electrically active magnon excitation, leading to the gigantic NDD in the terahertz region.

Optical ME effects are ensured in two representative geometries based on the macroscopic symmetry of matter [24,25]. When the electric polarization \mathbf{P} is perpendicular to the magnetization \mathbf{M} , the light propagating parallel to $\mathbf{P} \times \mathbf{M}$, i.e., $\mathbf{k}^\omega \parallel \mathbf{P} \times \mathbf{M}$, shows NDD. On the other hand, any chiral matter with magnetization \mathbf{M} exhibits NDD for light propagating parallel to \mathbf{M} , which is specifically referred to as the magnetochiral (MCh) effect. The helimagnets can induce both OME effects irrespective of the underlying lattice symmetry. For example, the transverse conical spin structure, which shows the ferroelectric polarization \mathbf{P} as shown in Fig. 1(b), provides the OME effect for light propagating along $\mathbf{P} \times \mathbf{M}$, i.e., parallel to the magnetic modulation vector \mathbf{q}_m . In this geometry, the electromagnon with the characteristics of the transverse fluctuation mode of \mathbf{P} is excited by light with $\mathbf{E}^\omega \perp \mathbf{P}$, so that the enhanced OME effect can be expected in the terahertz response of electromagnon resonance [16,19,30]. On the other hand, the MCh effect is realized by the longitudinal conical spin structure [see Fig. 1(c)], where the helicity of the proper screw-spin component is responsible for the chirality. Accordingly, the light propagating parallel to \mathbf{M} , i.e., $\mathbf{k}^\omega \parallel \mathbf{M} \parallel \mathbf{q}_m$, shows the OME effect [20,30]. The ME

*narita@issp.u-tokyo.ac.jp

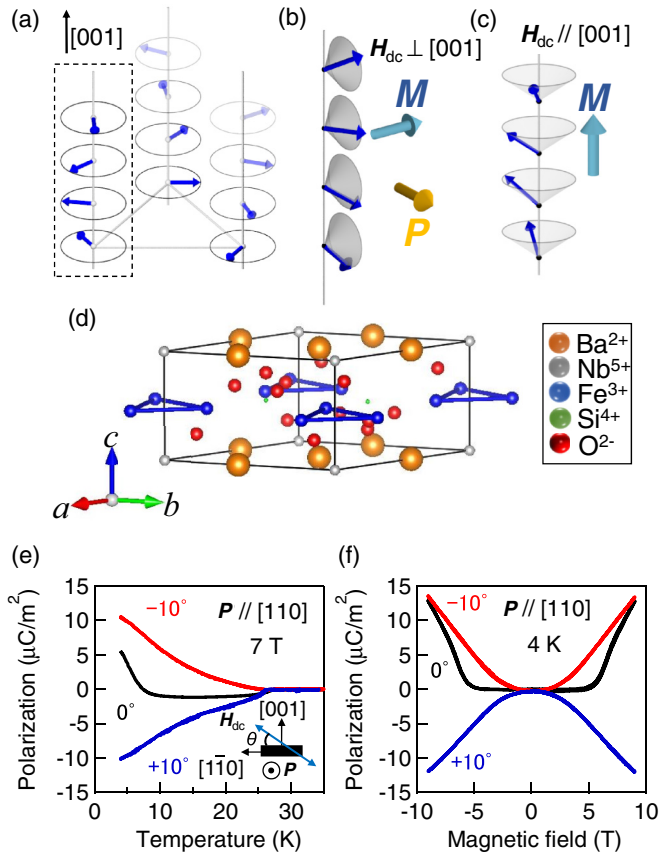


FIG. 1. (a) Schematic of the spin structure of BNSFO in the screw-spin phase. (b) Schematic of the spin chain constituent of BNSFO [dotted square in Fig. 1(a)] under a magnetic field perpendicular to [001]. The induced magnetization M and orthogonal ferroelectric polarization P are indicated. (c) Conical screw-spin chain under a magnetic field along the [001] axis. (d) Crystal structure of BNSFO. (e) Temperature dependence of the ferroelectric polarization along the [110] axis under the magnetic field parallel to [110] and with slight inclination with respect to [110]. Inset shows the experimental geometry of the magnetic field and ferroelectric polarization. (f) Magnetic-field dependence of ferroelectric polarization with the same experimental configuration as with Fig. 1(e). As seen in (e) and (f) the sign of magnetic-field-induced P is reversed between $\theta = -10^\circ$ and 10° , reflecting the helicity reversal of the induced cycloidal component.

response of the electromagnon resonance is also explained by the SC mechanism; the uniform fluctuation of the conical spin structure induces the oscillation of electric polarization, resulting in dynamical ME coupling with the electromagnetic field of light [31,32]. Therefore, the helimagnet is a promising candidate not only for the ME multiferroics, but also for the novel OME effect in the terahertz region.

The iron-based langasite $\text{Ba}_3\text{NbFe}_3\text{Si}_2\text{O}_{14}$ (BNFSO) investigated in this paper belongs to the $P321$ chiral trigonal space group in the paramagnetic phase. The spins on Fe^{3+} ions ($S = 5/2$) are responsible for the magnetism. Below $T_N = 27$ K, iron spins form a proper screw-helical magnetic structure along the [001] axis with an incommensurate magnetic modulation vector close to $(0, 0, \sim 1/7)$ owing to the frustration of

exchange interactions [see Fig. 1(a)] [33]. On the other hand, the in-plane triangular lattice also possesses a geometrical frustration as shown in Fig. 1(d), leading to the 120° spin structure. One distinct feature of the BNFSO compound is a strong correlation between the structural chirality and helicity/chirality of magnetism. In an enantiopure crystal, one of two helicities for screw spins is exclusively selected because of the chiral exchange pass induced by the chiral atomic configuration. Furthermore, the rotation angle of the 120° spin structure on the triangular lattice is also fixed at either $+120^\circ$ or -120° owing perhaps to the DM interactions, as shown in Fig. 1(a) [33,34]. Thus, the enantiomorphic single crystal provides an automatically selected single domain for the two distinct chiral spin orders, i.e., the 120° spin order in the in-plane triangular lattice and the screw-spin order along the [001] axis.

In this paper, we have investigated OME effects on the electromagnon resonance of BNFSO by time-domain terahertz spectroscopy, which allows us to perform a high-quality polarimetry experiment. The NDD on the electromagnon resonance was examined in the helimagnetic spin phase for two distinct configurations including the MCh effect. Although the MCh effect is always allowed by the structural chirality of langasite compounds, the pronounced NDD on the electromagnon resonance occurs only in the helimagnetic spin phase. In addition, the formation of helimagnetic spin order was found to cause the enhanced natural optical activity in cooperation with the structural chirality.

II. EXPERIMENTS

A single crystal of $\text{Ba}_3\text{NbFe}_3\text{Si}_2\text{O}_{14}$ (BNFSO) was grown using the floating-zone method. The sample was characterized by the measurements of magnetization (data not shown) and the electric polarization, the latter of which was obtained by time integration of polarization current with use of an electrometer (6517B, Keithley) while sweeping the temperature or magnetic field without any preliminary ME poling procedure. The (001) plane sample with dimensions of $5 \times 5 \times 2$ mm³ was prepared for terahertz transmittance spectroscopy. Time-domain terahertz spectroscopy was performed under magnetic fields (0–7 T) by using superconducting magnets [35]. A magnetic field was applied perpendicular to (Voigt geometry) or parallel to (Faraday geometry) the propagation vector of light (\mathbf{k}^ω). The complex refractive indices were calculated through complex transmission without using the Kramers-Kronig transformation. A femtosecond laser (Spectra-Physics Mai Tai; a mode-locked Ti:sapphire laser with 800 nm center wavelength, 100 fs pulse width, and 80 MHz repetition rate) was used to generate and detect the terahertz pulse. A bowtie-shaped photoconductive antenna was used to generate the terahertz pulses, and a dipole-shaped photoconductive antenna was used to detect the waveform of terahertz pulses. In the Faraday geometry, the complex transmittances measured with a wire-grid polarizer oriented at $+45^\circ$ or -45° with respect to the detector allowed us to calculate the complex refractive indices on the circular polarization bases.

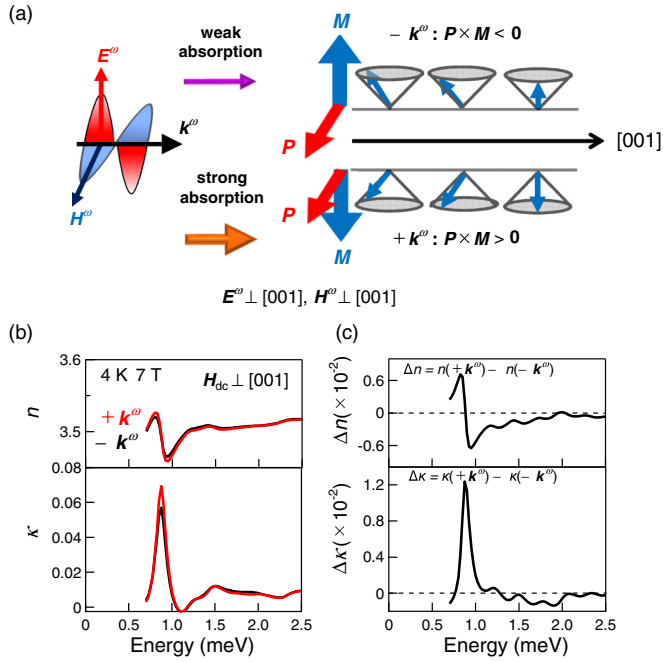


FIG. 2. (a) The experimental geometry of light polarization ($E^\omega \perp P$), ferroelectric polarization P , magnetization M , and spin structures for two different states in terms of the OME effect. (b) Complex refractive indices for different states in terms of the OME effect, as indicated by $+k^\omega$ and $-k^\omega$ [see text and Fig. 2(a) for definition] at 4 K under an external magnetic field (7 T). (c) Complex OME spectra (Δn and $\Delta \kappa$) derived from Fig. 2(b).

III. RESULTS

A. NDD in Voigt geometry

First, we demonstrate NDD via electromagnon resonance in Voigt geometry ($k^\omega \perp H_{dc}$). Because a single helical spin domain is ensured by the crystal chirality, spin-driven ferroelectric polarization occurs under the magnetic field ($H_{dc} \perp [001]$) below T_N owing to the cycloidal spin component, as shown in Figs. 1(e) and 2(a) [36]. Therefore, the orthogonal configuration of the ferroelectric polarization P and magnetization M can be prepared without an external electric field [see Fig. 1(b)]. The NDD is expressed by the addition of the ME term $N_{ME}(\omega)$ to the ordinary term of the complex refractive index $n_O(\omega) + i\kappa_O(\omega)$ as follows:

$$n(\omega, k^\omega, P, M) + i\kappa(\omega, k^\omega, P, M) \\ = [n_O(\omega) + i\kappa_O(\omega)] + \text{sgn}(k^\omega \cdot (P \times M))N_{ME}(\omega). \quad (1)$$

The coefficient of $N_{ME}(\omega)$ is determined by the sign of $k^\omega \cdot (P \times M)$ such that the reversal of either P or M causes the sign change of the coefficient of $N_{ME}(\omega)$ as well as the reversal of k^ω . Since ferroelectric polarization has a form of even function of the magnetic field in BNSFO [see Fig. 1(f)], the reversal of M results in the sign change of $P \times M$, as shown in Fig. 2(a). Hereafter, we denote these different states in terms of the OME effect by $+k^\omega$ and $-k^\omega$.

The real (n) and imaginary (κ) parts of the complex refractive indices at 4 K and 7 T are shown in Fig. 2(b). Clear magnetic resonance is observed at 0.9 meV in addition to the weak absorption between 1.5 and 2.0 meV, in accordance

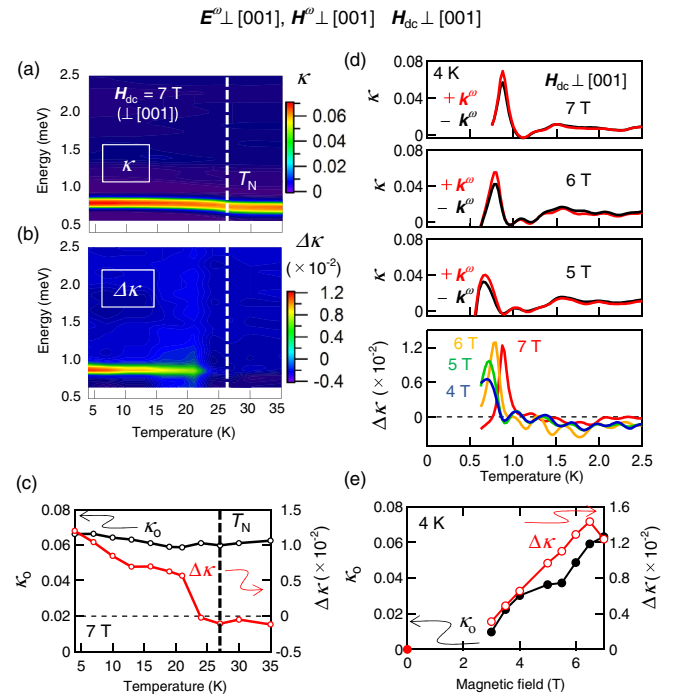


FIG. 3. Temperature dependence of (a) extinction coefficient (κ) and (b) OME spectra ($\Delta \kappa$) at 7 T. (c) Temperature dependence of the peak magnitudes of OME effect ($\Delta \kappa$) and ordinary term of extinction coefficient (κ_O). The intensity of κ_O is defined as $[\kappa(+k^\omega) + \kappa(-k^\omega)]/2$. (d) Magnetic-field dependence of extinction coefficient (κ) and OME spectra ($\Delta \kappa$) at 4 K. (e) Magnetic-field dependence of peak magnitudes of OME effect ($\Delta \kappa$) and ordinary term (κ_O) at 4 K.

with electron spin resonance (ESR) measurement [34] and far-infrared spectroscopy [37,38]. The distinct 0.9 meV mode shows pronounced NDD as large as 20% of the parent resonance. The ME spectra, which are defined by the difference of spectra for $+k^\omega$ and $-k^\omega$, exhibit a sharp resonance on the 0.9 meV mode, as manifested by the dispersive structure in Δn and the resonance peak in $\Delta \kappa$ [Fig. 2(c)]. A weak NDD is also observed around 1.8 meV with opposite sign to the 0.9 meV mode, indicating the appreciable amount of ME coupling on this higher-lying mode as well. Thus, both modes possess the electric-dipole as well as the magnetic-dipole activities, showing the character of electromagnon.

Figures 3(a) and 3(b) show the temperature dependences of magnetic resonance (κ) and NDD ($\Delta \kappa$) at 7 T. The lower-lying mode persists with increasing temperature above T_N , while a slight decrease of resonance energy is discerned at T_N . In contrast, the NDD ($\Delta \kappa$) on the 0.9 meV mode vanishes upon transition from the helical spin phase to the paramagnetic phase at T_N ($=27$ K), as shown in Figs. 3(b) and 3(c). Thus, the formation of helical spin order is responsible for the OME effect. This result is also consistent with the symmetry consideration because P disappears in the paramagnetic phase [see Fig. 1(e)] such that $P \times M = 0$. Figures 3(d) and 3(e) show the magnetic-field dependence of κ and $\Delta \kappa$. Peak intensities of the 0.9 meV mode show strong magnetic-field dependence, where the magnetization is proportional to the magnetic field.

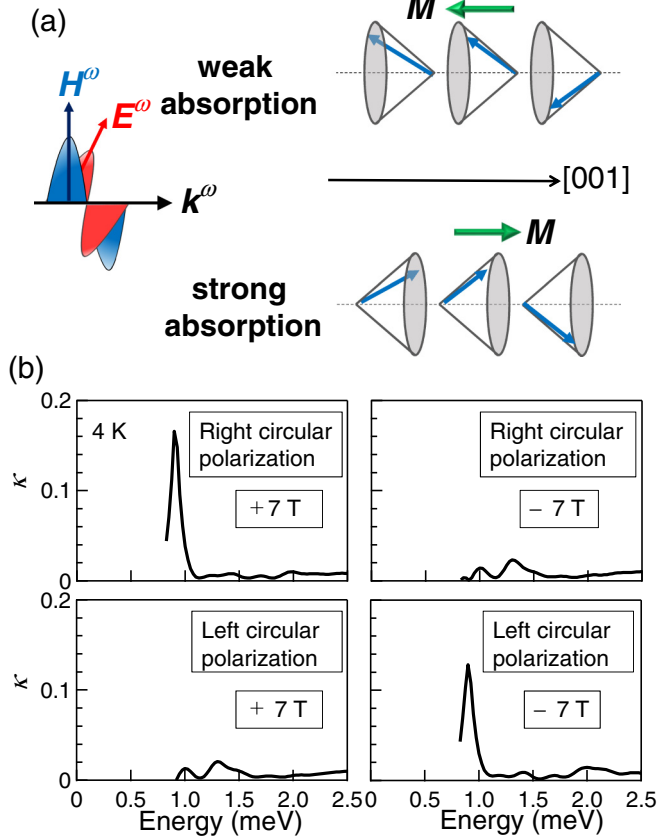


FIG. 4. (a) The experimental geometry of light polarization ($\mathbf{E}^\omega \perp \mathbf{P}$), magnetization \mathbf{M} , and spin structures for two different states in terms of the MCh effect; the helicity of the screw spins are the same, but their magnetizations are opposite. (b) Extinction coefficients for right- and left-circular polarizations under magnetic fields of +7 T and -7 T at 4 K.

As shown in Fig. 3(e), a monotonous increase of the OME effect ($\Delta\kappa$) with magnetic field is observed, indicating that the increase of \mathbf{P} as well as \mathbf{M} , i.e., the magnitude of $\mathbf{P} \times \mathbf{M}$, plays a crucial role in the OME effect, as expected.

B. MCh effect and optical activities in Faraday geometry

The Faraday geometry, where the magnetic field is parallel to the propagation vector of light, allows us to access another OME effect in chiral matter, i.e., the MCh effect. The screw-spin structure is expected to produce the MCh effect on the electromagnon resonance when the magnetic field is parallel to the screw axis [31,32]. To observe this phenomenon, we applied a magnetic field along [001], as shown in Figs. 1(c) and 4(a). In order to separate the MCh effect from possible optical activities, including natural optical activity and magnetic optical activity (Faraday effect), we employed the terahertz polarimetry technique. Since the propagation direction of light is fixed to $+\mathbf{k}^\omega$ in our measurement, four spectra, i.e., $N_{L/R}(\omega, +\mathbf{k}^\omega, \pm\mathbf{M})$, were measured independently as shown in Fig. 4(b), where L and R indicate the left- and right-handed circularly polarized light. This polarimetry enables us to separate all the independent optical terms for the enantiopure crystal, such as the MCh effect [$N_{\text{MCh}}(\omega)$], natural optical activity [$N_{\text{NOA}}(\omega)$], magnetic optical activity [$N_{\text{MOA}}(\omega)$], and ordinary term [$N_{\text{O}}(\omega)$], through the following relation:

$$\begin{aligned}
 N_{L/R}(\omega, \mathbf{k}^\omega, \mathbf{M}) &= \sqrt{\varepsilon(\omega, \mathbf{k}^\omega, \mathbf{M}, \boldsymbol{\beta}(\mathbf{L}/\mathbf{R}))\mu(\omega, \mathbf{k}^\omega, \mathbf{M}, \boldsymbol{\beta}(\mathbf{L}/\mathbf{R}))} \\
 &\quad + \text{sgn}(\mathbf{k}^\omega)\text{sgn}(\mathbf{M})N_{\text{MCh}}(\omega) \\
 &= N_{\text{O}}(\omega) + \boldsymbol{\beta}(\mathbf{L}/\mathbf{R})N_{\text{NOA}}(\omega) \\
 &\quad + \boldsymbol{\beta}(\mathbf{L}/\mathbf{R})\text{sgn}(\mathbf{M})N_{\text{MOA}}(\omega) \\
 &\quad + \text{sgn}(\mathbf{k}^\omega)\text{sgn}(\mathbf{M})N_{\text{MCh}}(\omega).
 \end{aligned} \tag{2}$$

Here, $\boldsymbol{\beta}(\mathbf{L}) = +1$ and $\boldsymbol{\beta}(\mathbf{R}) = -1$. We assumed that the cross terms between the natural and magnetic optical activities in the dielectric constant ε and magnetic permeability μ (in the form of $\sqrt{\varepsilon\mu}$) are negligibly small. In fact, the magnitude of the cross term, which is approximately described by $2N_{\text{MOA}}(\omega)N_{\text{NOA}}(\omega)$, is less than 10^{-3} in $\Delta\kappa$ and Δn in our experiments. Accordingly, all independent terms in refractive indices including $N_{\text{MCh}}(\omega)$, $N_{\text{MOA}}(\omega)$, and $N_{\text{NOA}}(\omega)$ can be calculated by Eq. (2) as follows:

$$\begin{aligned}
 N_{\text{O}}(\omega) &= \frac{N_{\text{L}}(\omega, +\mathbf{k}^\omega, +\mathbf{M}) + N_{\text{L}}(\omega, +\mathbf{k}^\omega, -\mathbf{M}) + N_{\text{R}}(\omega, +\mathbf{k}^\omega, +\mathbf{M}) + N_{\text{R}}(\omega, +\mathbf{k}^\omega, -\mathbf{M})}{4}, \\
 N_{\text{MOA}}(\omega) &= \frac{N_{\text{L}}(\omega, +\mathbf{k}^\omega, +\mathbf{M}) - N_{\text{L}}(\omega, +\mathbf{k}^\omega, -\mathbf{M}) - N_{\text{R}}(\omega, +\mathbf{k}^\omega, +\mathbf{M}) + N_{\text{R}}(\omega, +\mathbf{k}^\omega, -\mathbf{M})}{4}, \\
 N_{\text{NOA}}(\omega) &= \frac{N_{\text{L}}(\omega, +\mathbf{k}^\omega, +\mathbf{M}) + N_{\text{L}}(\omega, +\mathbf{k}^\omega, -\mathbf{M}) - N_{\text{R}}(\omega, +\mathbf{k}^\omega, +\mathbf{M}) - N_{\text{R}}(\omega, +\mathbf{k}^\omega, -\mathbf{M})}{4}, \\
 N_{\text{MCh}}(\omega) &= \frac{N_{\text{L}}(\omega, +\mathbf{k}^\omega, +\mathbf{M}) - N_{\text{L}}(\omega, +\mathbf{k}^\omega, -\mathbf{M}) + N_{\text{R}}(\omega, +\mathbf{k}^\omega, +\mathbf{M}) - N_{\text{R}}(\omega, +\mathbf{k}^\omega, -\mathbf{M})}{4}.
 \end{aligned} \tag{3}$$

The resultant spectra for these terms are summarized in Figs. 5 and 6.

A clear magnetic resonance is observed at 0.9 meV and 7 T [see Fig. 4(b) and Fig. 5], which is consistent with the reported ESR measurement [34]. The magnitudes of the ordinary term and of magnetic optical activity for the resonance around

0.9 meV are comparable, as shown in Figs. 5(a) and 5(b); therefore, this resonance is almost circularly polarized [see also Fig. 4(b)]. In addition, we observed the MCh effect and the natural optical activity on the resonance, as shown in Figs. 5(c) and 5(d). The presence of the MCh effect proves the electromagnon character for this resonance because the

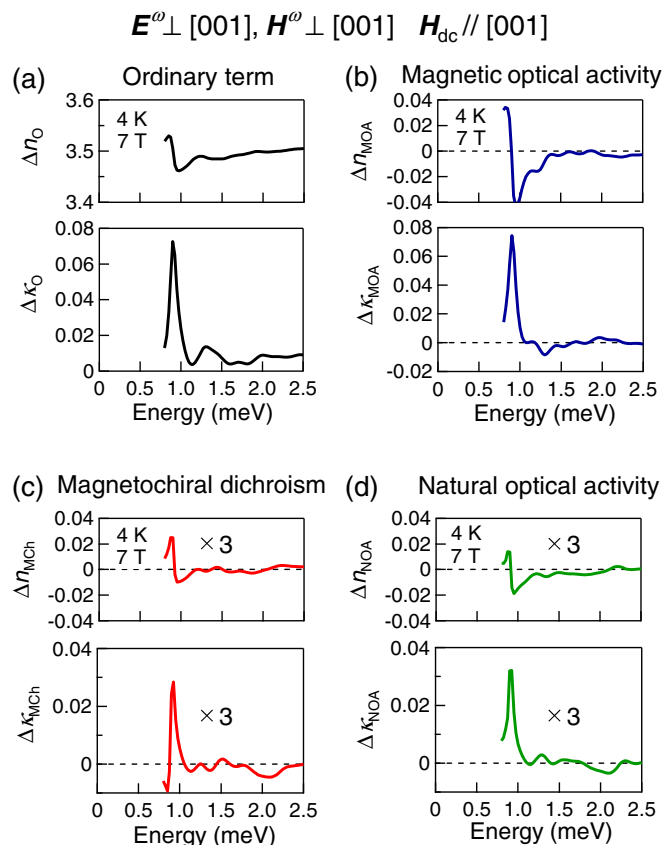


FIG. 5. Complex refractive indices (Δn and $\Delta \kappa$) for independent optical activities (effect) derived from Fig. 4(b) with the use of Eq. (3). (a) Ordinary term ($N_O = \Delta n_O + i\Delta \kappa_O$), (b) magnetic optical activity ($N_{MOA} = \Delta n_{MOA} + i\Delta \kappa_{MOA}$), (c) MCh effect ($N_{MCh} = \Delta n_{MCh} + i\Delta \kappa_{MCh}$), and (d) natural optical activity ($N_{NOA} = \Delta n_{NOA} + i\Delta \kappa_{NOA}$) [see text and Eq. (2) and (3) for definition].

electric-dipole transition moment is indispensable for the OME effect including the MCh effect. Their magnitudes are as large as 15% of the ordinary term and of the magnetic optical activity. Thus, the magnetic resonance at 0.9 meV shows all the possible optical effects related to the circular polarization dichroism below T_N .

Figure 6 summarizes the temperature dependence of these terms at 7 T. In Fig. 6(a), the temperature dependence of the normalized peak intensity by the ordinary term ($N_O = \Delta n_O + i\Delta \kappa_O$) is plotted for the magnetic optical activity ($\Delta \kappa_{MOA}/\Delta \kappa_O$: MOA, circle), natural optical activity ($\Delta \kappa_{NOA}/\Delta \kappa_O$: NOA, triangle), and MCh effect ($\Delta \kappa_{MCh}/\Delta \kappa_O$: MCh, square). As shown in Figs. 6(b) and 6(c), the ordinary term and the magnetic optical activity show little temperature dependence throughout the measured temperature range (4–40 K), including the magnetic transition at $T_N = 27$ K. In contrast, the MCh effect [Fig. 6(d)] and the natural optical activity [Fig. 6(e)] are suppressed above T_N . Therefore, the formation of the helical spin order is responsible for the MCh effect and natural optical activity on the magnetic resonance at 0.9 meV. A difference in behavior between the MCh effect and natural optical activity was observed above T_N ; the magnitude of the MCh effect decreases to nearly zero, while a finite natural

optical activity is observed above T_N , as should be allowed by the lattice-chiral symmetry.

IV. DISCUSSION

In BNFSO, two distinguishable spin orders coexist: the 120° spin structure in the in-plane triangular lattice and the screw-spin structure along [001] axis [see Fig. 1(a)]. The “vector spin chirality” defined by sum of $S_i \times S_j$ has been discussed in the frustrated spin system including multiferroics [7], which is to be distinguished from “electronic chirality” characterized by the breaking of space inversion and mirror symmetries. (Note here that the term “electronic chirality” is used to refer to conventional chirality produced by the chiral-lattice structure and/or helical spin structure to distinguish it from the “vector spin chirality.”) The vector spin chirality of the 120° spin structure on one triangular lattice, which is described by $(S_1 \times S_2) + (S_2 \times S_3) + (S_3 \times S_1)$ for triangular-site spins $S_{1,2,3}$, has a finite value; the net vector spin chirality of them can also acquire a finite value for a chiral-lattice magnet [39]. A single domain for the vector spin chirality on the triangular lattice as well as for the helical spin structure is formed owing to the structural chirality in BNFSO [33]. It should be emphasized that the sign of the vector spin chirality derived from the 120° spin structure is invariant for the mirror operation with respect to the spin-site plane, while the electronic chirality, i.e., the helicity of the screw, is reversed. Therefore, the vector spin chirality on triangular lattice is considered to be less important for the natural optical activity and the MCh effect, which are allowed under the presence of electronic chirality.

The MCh effect on the magnetic resonance clearly shows the correlation with the magnetic order, as shown in Fig. 6(a), while the MCh effect is always allowed by symmetry owing to the lattice-structural chirality. Accordingly, the formation of the screw-spin structure is responsible for the presence of the MCh effect on the electromagnon resonance, as explained by the dynamical ME coupling through the SC model [20,31]. In fact, early works demonstrated the pronounced MCh effect of the electromagnon resonance on the screw-spin helimagnets $\text{CuFe}_{1-x}\text{Ga}_x\text{O}_2$ ($x = 0.035$) [20] and MnWO_4 [30].

Another noteworthy result is the change in magnitude of natural optical activity on the magnetic resonance; the finite polarization rotation in the paramagnetic phase is enhanced in the screw-spin phase, as shown in Fig. 6(a). Large magnetic-field-induced natural optical activity has been reported on the spin excitation in $\text{Ba}_2\text{CoGe}_2\text{O}_7$ [17] and on the $d-d$ transition in CuB_2O_4 [23], in which both the external magnetic field and underlying crystal symmetry (i.e., point group $\bar{4}2m$) are responsible for the presence of the electronic chirality. In the case of $\text{Ba}_2\text{CoGe}_2\text{O}_7$, the diagonal term of the ME tensor was assigned to the origin of the natural optical activity on the spin excitation in the terahertz region [17]. The optical activity, i.e., polarization rotation, driven by the diagonal term of the ME tensor was also reported for another chiral-lattice magnet $\text{SmFe}_3(\text{BO}_3)_4$ in the gigahertz and terahertz region [40]. In BNFSO, by contrast, the crystal structure should lead to electronic chirality such that the natural optical activity is always allowed by the off-diagonal term of the dielectric

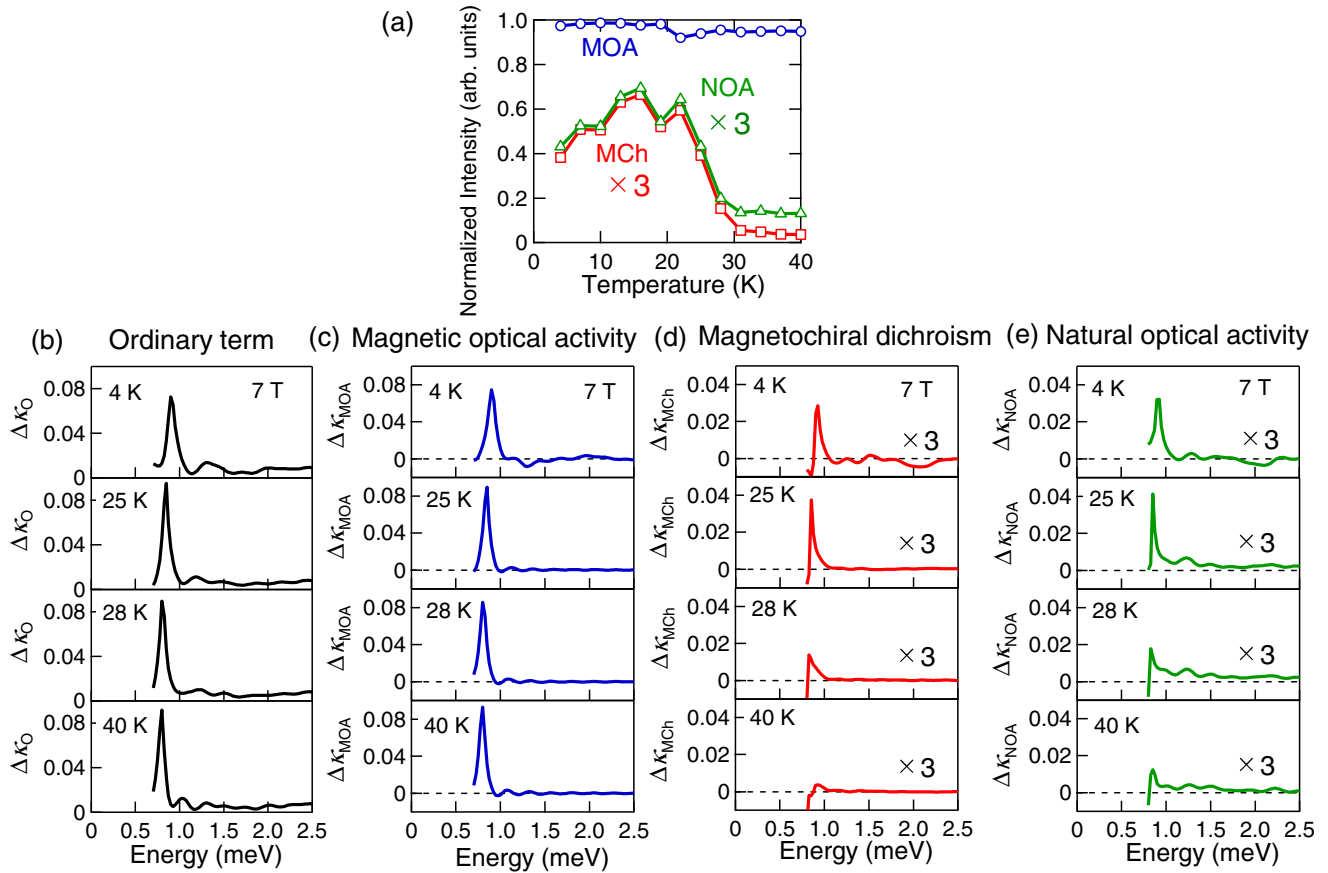


FIG. 6. (a) Temperature dependences of the peak intensities for magnetic optical activity ($\Delta\kappa_{MOA}/\Delta\kappa_O$: MOA, circle), natural optical activity ($\Delta\kappa_{NOA}/\Delta\kappa_O$: NOA, triangle), and MCh effect ($\Delta\kappa_{MCh}/\Delta\kappa_O$: MCh, square) normalized by the ordinary term $\Delta\kappa_O$ at 7 T. Temperature dependences of (b) ordinary term, (c) magnetic optical activity, (d) MCh effect, and (e) natural optical activity at 7 T.

constant and magnetic permeability. Under the magnetic field along the [001] axis, the crystal space group $P321$ turns into $32'$ in the magnetic point group, in which the diagonal elements of the ME tensor are zero and the nonzero off-diagonal elements are responsible for the MCh effect. (Note that we assume the space group of the crystal in the paramagnetic phase, although the lowering of symmetry has been discussed in the magnetically ordered phase at lower temperatures [38,41].) Therefore, the natural optical activity on the magnetic resonance can be ascribed to the off-diagonal elements of the dielectric constant and/or of the magnetic permeability. The enhancement of the natural optical activity on the magnetic resonance [see Fig. 6(a)] may be caused by the electromagnon character itself, which allows for the additional contribution to the natural optical activity through the dielectric part.

V. CONCLUSION

In conclusion, we have demonstrated NDD via electromagnon resonance in the chiral magnet $\text{Ba}_3\text{NbFe}_3\text{Si}_2\text{O}_{14}$ by using time-domain terahertz spectroscopy. The single helicity domain of the screw-spin structure, which is ensured by the

structural chirality, enabled us to measure the OME effect without the ME cooling process. In Voigt geometry, the OME effect on the electromagnon resonance was observed in the screw-spin phase, as indicated by NDD as high as 20% of the parent resonance. In Faraday geometry, the magnetic optical activity, natural optical activity, and MCh effect could be separately detected by using terahertz polarimetry. The MCh effect was observed in the screw-spin phase, indicating the dynamical ME coupling through the SC mechanism. The natural optical activity is also enhanced upon the formation of the screw-spin order, suggesting the important role of electromagnon resonance not only in the ME tensor but also in the dielectric-constant tensor. In contrast, the magnetic optical activity remains almost unchanged upon the transition to the screw-spin order. These results show that the various characters coexist on the magnetic resonance in the chiral-lattice magnet.

ACKNOWLEDGMENT

This paper was partly supported by the Japan Society for the Promotion of Science (JSPS) Grants-in-Aid for Scientific Research (No. 26706011 and No. 24224009).

[1] G. H. Wagniere, *On Chirality and the Universal Asymmetry* (Wiley-VCH, Zurich, Weinheim, 2007).

[2] S. Mühlbauer, B. Binz, F. Jonietz, C. Pfleiderer, A. Rosch, A. Neubauer, R. Georgii, and P. Böni, *Science* **323**, 915 (2009).

- [3] X. Z. Yu, Y. Onose, N. Kanazawa, J. H. Park, J. H. Han, Y. Matsui, N. Nagaosa, and Y. Tokura, *Nature (London)* **465**, 901 (2010).
- [4] Y. Togawa, T. Koyama, K. Takayanagi, S. Mori, Y. Kousaka, J. Akimitsu, S. Nishihara, K. Inoue, A. S. Ovchinnikov, and J. Kishine, *Phys. Rev. Lett.* **108**, 107202 (2012).
- [5] W. Eerenstein, N. D. Mathur, and J. F. Scott, *Nature (London)* **442**, 759 (2006).
- [6] J. F. Scott, *Science* **315**, 954 (2007).
- [7] Y. Tokura, S. Seki, and N. Nagaosa, *Rep. Prog. Phys.* **77**, 076501 (2014).
- [8] T. Kimura, T. Goto, H. Shintani, K. Ishizaka, T. Arima, and Y. Tokura, *Nature* **426**, 55 (2003).
- [9] H. Katsura, N. Nagaosa, and A. V. Balatsky, *Phys. Rev. Lett.* **95**, 057205 (2005).
- [10] M. Mostovoy, *Phys. Rev. Lett.* **96**, 067601 (2006).
- [11] I. A. Sergienko and E. Dagotto, *Phys. Rev. B* **73**, 094434 (2006).
- [12] H. Murakawa, Y. Onose, K. Ohgushi, S. Ishiwata, and Y. Tokura, *J. Phys. Soc. Jpn.* **77**, 043709 (2008).
- [13] L. D. Barron, *Molecular Light Scattering and Optical Activity* (Cambridge University Press, Cambridge, UK, 2004).
- [14] T. Arima, *J. Phys. Condens. Matter* **20**, 434211 (2008).
- [15] I. Kézsmárki, N. Kida, H. Murakawa, S. Bordács, Y. Onose, and Y. Tokura, *Phys. Rev. Lett.* **106**, 057403 (2011).
- [16] Y. Takahashi, R. Shimano, Y. Kaneko, H. Murakawa, and Y. Tokura, *Nat. Phys.* **8**, 121 (2012).
- [17] S. Bordács, I. Kézsmárki, D. Szaller, L. Demkó, N. Kida, H. Murakawa, Y. Onose, R. Shimano, T. Rőöm, U. Nagel, S. Miyahara, N. Furukawa, and Y. Tokura, *Nat. Phys.* **8**, 734 (2012).
- [18] Y. Okamura, F. Kagawa, M. Mochizuki, M. Kubota, S. Seki, S. Ishiwata, M. Kawasaki, Y. Onose, and Y. Tokura, *Nat. Commun.* **4**, 2391 (2013).
- [19] Y. Takahashi, Y. Yamasaki, and Y. Tokura, *Phys. Rev. Lett.* **111**, 037204 (2013).
- [20] S. Kibayashi, Y. Takahashi, S. Seki, and Y. Tokura, *Nat. Commun.* **5**, 4583 (2014).
- [21] G. L. J. A. Rikken, C. Strohm, and P. Wyder, *Phys. Rev. Lett.* **89**, 133005 (2002).
- [22] M. Saito, K. Ishikawa, and T. Arima, *J. Phys. Soc. Jpn.* **77**, 013705 (2008).
- [23] M. Saito, K. Ishikawa, K. Taniguchi, and T. Arima, *Phys. Rev. Lett.* **101**, 117402 (2008).
- [24] G. L. J. A. Rikken and E. Raupach, *Nature (London)* **390**, 493 (1997).
- [25] T. Roth and G. L. J. A. Rikken, *Phys. Rev. Lett.* **88**, 063001 (2002).
- [26] C. Train, R. Gheorghe, V. Krstic, L.-M. Chamoreau, N. S. Ovanesyan, G. L. J. A. Rikken, M. Gruselle, and M. Verdaguer, *Nat. Mater.* **7**, 729 (2008).
- [27] R. Sessoli, M.-E. Boulon, A. Caneschi, M. Mannini, L. Poggini, F. Wilhelm, and A. Rogalev, *Nat. Phys.* **11**, 69 (2014).
- [28] B. Pelle, H. Bitard, G. Bailly, and C. Robilliard, *Phys. Rev. Lett.* **106**, 193003 (2011).
- [29] N. Kida, H. Yamada, H. Sato, T. Arima, M. Kawasaki, H. Akoh, and Y. Tokura, *Phys. Rev. Lett.* **99**, 197404 (2007).
- [30] Y. Takahashi, S. Kibayashi, Y. Kaneko, and Y. Tokura, *Phys. Rev. B* **93**, 180404(R) (2016).
- [31] S. Miyahara and N. Furukawa, *J. Phys. Soc. Jpn.* **81**, 023712 (2012).
- [32] S. Miyahara and N. Furukawa, *Phys. Rev. B* **89**, 195145 (2014).
- [33] K. Marty, V. Simonet, E. Ressouche, R. Ballou, P. Lejay, and P. Bordet, *Phys. Rev. Lett.* **101**, 247201 (2008).
- [34] A. Zorko, M. Pregelj, A. Potočnik, J. van Tol, A. Ozarowski, V. Simonet, P. Lejay, S. Petit, and R. Ballou, *Phys. Rev. Lett.* **107**, 257203 (2011).
- [35] N. Kida, Y. Ikebe, Y. Takahashi, J. P. He, Y. Kaneko, Y. Yamasaki, R. Shimano, T. Arima, N. Nagaosa, and Y. Tokura, *Phys. Rev. B* **78**, 104414 (2008).
- [36] N. Lee, Y. J. Choi, and S.-W. Cheong, *Appl. Phys. Lett.* **104**, 072904 (2014).
- [37] L. Chaix, S. de Brion, F. Lévy-Bertrand, V. Simonet, R. Ballou, B. Canals, P. Lejay, J. B. Brubach, G. Creff, F. Willaert, P. Roy, and A. Cano, *Phys. Rev. Lett.* **110**, 157208 (2013).
- [38] C. Toulouse, M. Cazayous, S. de Brion, F. Levy-Bertrand, H. Barkaoui, P. Lejay, L. Chaix, M. B. Lepetit, J. B. Brubach, and P. Roy, *Phys. Rev. B* **92**, 104302 (2015).
- [39] H. Mitamura, R. Watanuki, K. Kaneko, N. Onozaki, Y. Amou, S. Kittaka, R. Kobayashi, Y. Shimura, I. Yamamoto, K. Suzuki, S. Chi, and T. Sakakibara, *Phys. Rev. Lett.* **113**, 147202 (2014).
- [40] A. M. Kuzmenko, A. Shuvaev, V. Dziom, Anna Pimenov, M. Schiebl, A. A. Mukhin, V. Yu. Ivanov, L. N. Bezmaternykh, and A. Pimenov, *Phys. Rev. B* **89**, 174407 (2014).
- [41] I. S. Lyubutin, P. G. Naumov, B. V. Mill', K. V. Frolov, and E. I. Demikhov, *Phys. Rev. B* **84**, 214425 (2011).